



1 **Atmospheric CO₂ inversions at the mesoscale using data driven**
2 **prior uncertainties. Part2: the European terrestrial CO₂ fluxes**

3

4 Panagiotis Kountouris¹, Christoph Gerbig¹, Christian Rödenbeck¹, Ute Karstens^{1,*}, Thomas F.
5 Koch², Martin Heimann¹

6 ¹Max Planck Institute for Biogeochemistry, Jena, Germany

7 ²Meteorological Observatory Hohenpeissenberg, Deutscher Wetterdienst, Germany

8 *now at ICOS Carbon Portal, Lund University, Lund, Sweden

9

10 *Correspondence to:* P. Kountouris (pkount@bgc-jena.mpg.de)

11

12

13

14

15

16

17

18

19

20

21



1 **Abstract**

2

3 Optimized biogenic carbon fluxes for Europe were estimated from high resolution regional scale
4 inversions, utilizing atmospheric CO₂ measurements at 16 stations for the year 2007. Additional
5 sensitivity tests with different data-driven error structures were performed. As the atmospheric
6 network is rather sparse and consequently contains large spatial gaps, we use a priori biospheric
7 fluxes to further constrain the inversions. The biospheric fluxes were simulated by the
8 Vegetation Photosynthesis and Respiration Model (VPRM) at a resolution of 0.1° and optimized
9 against Eddy covariance data. Overall we estimate an a priori uncertainty of 0.54 GtC y⁻¹ related
10 to the poor spatial representation between the biospheric model and the ecosystem sites. The sink
11 estimated from the atmospheric inversions for the area of Europe (as represented in the model
12 domain) ranges between 0.23 and 0.38 GtC y⁻¹ (0.30 and 0.49 GtC y⁻¹ up-scaled to geographical
13 Europe). This is within the range of posterior flux uncertainty estimates of previous studies using
14 ground based observations.

15

16

17

18

19

20

21

22

23

24

25



1 **1 Introduction**

2

3 Global and regional atmospheric inversions have been applied using atmospheric CO₂
4 measurements made by a global network since two decades to infer terrestrial carbon fluxes
5 using surface in situ or flask measurements of CO₂ dry mole fractions. The optimization of CO₂
6 biospheric fluxes for the European domain has been the focus of interest in previous studies
7 either using pseudo or real data (Gurney et al., 2004; Peters et al., 2010; Carouge et al., 2010a;
8 Carouge et al., 2010b; Rivier et al., 2010; Broquet et al., 2011; Broquet et al., 2013; Peylin et al.,
9 2013). Retrieved fluxes from most of the inversions are obtained from global systems at coarse
10 resolution which makes difficult to retrieve the spatial and temporal flux variability at finer
11 scales. Large uncertainties in the flux retrievals are introduced due to the coarse resolution of the
12 transport models used and due to the network sparseness (Peters et al., 2010). For example the
13 prevailing westerly winds and the fact that all atmospheric sites are mainly located in central
14 Europe, introduce large flux uncertainties at eastern European regions.

15 Apart from ground based observations, satellite measurements have also been recently used in
16 atmospheric inversions to infer terrestrial fluxes (Basu et al., 2013; Deng et al., 2014; Chevallier
17 et al., 2014). The advantage of using space-borne measurements lies on the high density of the
18 observations providing the opportunity to constrain regions which the ground network does not
19 see. However satellite based inversions significantly differ from ground based inversions,
20 reporting a larger annual uptake for Europe. A characteristic example is the estimated European
21 uptake in the study by Reuter et al. (2014). They calculated an uptake of 1.02 GtCy⁻¹ which
22 triggered an ongoing debate on whether those estimates are data driven or they lack robustness
23 due to deficiencies in the satellite observations and in the inverse modeling (Feng et al., 2016).

24 One of the largest sources of uncertainty in inversions is the atmospheric transport uncertainty.
25 Modeled tracer dry mole fractions are biased particularly due to uncertainties of vertical mixing
26 near the surface (Gurney et al., 2003; Gerbig et al., 2008; Houweling et al., 2010). As a
27 consequence, posterior flux estimates are also biased because biases in concentrations are
28 translated into biases in fluxes through the optimization procedure. Propagation of uncertainties
29 in winds (Lin and Gerbig, 2005) and in mixing heights (Gerbig et al., 2008) for summer months



1 with active vegetation resulted in uncertainties in simulated dry air mole fractions of 5.9 ppm and
2 3.5 ppm respectively.

3 The current study is a continuation of the Kountouris et al. (2016) study (hereafter referred to as
4 Ko16) in which the inversion system and its set-up were assessed based on pseudo data. As a
5 next step we apply the modeling framework to real CO₂ atmospheric observations. Our main
6 objectives in the second part of this work are to investigate the potential to infer flux estimates
7 for Europe with reduced uncertainties, and to estimate biospheric fluxes at high spatial resolution
8 and for a full year. We use a spatial flux resolution of 0.25° x 0.25°, and the state space allows
9 optimizing 3-hourly NEE corrections to the prior NEE fluxes at a nominal spatial resolution of
10 0.5° x 0.5°. A data driven error structure is implemented consistent with model-data flux
11 mismatches (Kountouris et al., 2015) as tested in part 1 (Ko16) of this study. Further, different
12 error structures are used and assessed including also a spatial error structure with a hyperbolic
13 correlation shape as suggested by Chevallier et al. (2012). Since spatial autocorrelations have
14 been found to be very short, the annual aggregated uncertainty over the European domain is
15 smaller than traditionally assumed (see also Ko16). The error inflation necessity and
16 implementation was addressed in Ko16 either by inflating the error covariance or, more
17 formally, by introducing a bias term. However the hyperbolic correlation shape suggested by
18 Chevallier et al. (2012) has a stronger impact from larger distances compared to the exponential
19 shape, leading to an aggregated uncertainty which does not require to be inflated. We perform
20 also a number of sensitivity tests to account for misrepresentation of the fossil fuel signal and
21 also for transport uncertainties due to vertical mixing.

22 This paper is structured as follows: Section 2 describes the inversion system, the network and
23 station data which are used and details the assumed error structure. Section 3 shows the results of
24 the goodness of fit, and the retrieved fluxes. The data fitting and the reliability of the posterior
25 fluxes are extensively discussed in section 4.

26

27



1 2 Methods

2 2.1 Two-step inversion

3

4 Real-data inversions require a nested inversion scheme, since observations contain also
5 contributions from regions outside of the Domain of Interest (DoI). As in part 1 of this study
6 (Ko16), the Jena Inversion System (Rödenbeck 2005) including the two-step nesting scheme
7 (Rödenbeck et al., 2009; Trusilova et al., 2010) was used. This scheme allows for combining
8 regional and global inversions within a consistent system. Here we only provide a brief
9 description as details are given in Rödenbeck et al. (2009) and Trusilova et al. (2010). The
10 atmospheric transport models TM3 (step 1) (Heimann and Körner, 2003) and STILT (step 2)
11 (Lin et al., 2003) were used for transport at the global and regional domain, respectively. For the
12 global runs, TM3 was used at a spatial resolution of 4° latitude x 5° longitude, driven by
13 meteorological fields from the ERA-Interim reanalysis produced by ECMWF (Dee et al., 2011).
14 The transport matrix for the regional inversions was identical to the one used for the synthetic
15 data study in part 1.

16 In the first step, a global inversion is performed using the global transport model. The outcome is
17 an optimized flux field, at coarser scale for the full period (FP) and the global domain. Then two
18 forward runs are performed. The first run uses the global transport model over the FP, computing
19 the modeled mixing ratios Δc_{mod1} . The second run initializes again the global transport model but
20 only within the regional DoI. This can be regarded as a regional simulation, but with coarse
21 resolution, yielding modeled mixing ratios Δc_{mod2} . Then the “remaining mixing ratio” is
22 calculated for all the observing sites inside the DoI:

$$23 \quad \Delta c_{remain} = c_{meas} - (\Delta c_{mod1} - \Delta c_{mod2} + c_{ini}) \quad (1)$$

24 were c_{ini} the initial condition which corresponds to a well mixed atmosphere with a given initial
25 tracer mixing ratio.

26 In step two, the high-resolution transport model is used for the regional inversion within the DoI,
27 where all fluxes are represented at fine resolution. For this inversion the vector containing the



1 measured mixing ratios c_{meas} are replaced by the “remaining mixing ratios” Δc_{remain} . The
2 optimized fluxes from this step are the high-resolution fluxes of interest.

3

4 **2.2 Atmospheric network and data**

5

6 For step 1 we used the same station network as in version s04_v3.6 of the Jena CarboScope CO₂
7 inversion (http://www.bgc-jena.mpg.de/CarboScope/?ID=s04_v3.6), with 64 stations globally. For
8 step 2 (regional inversion) continuous and flask measurements from 16 stations within Europe
9 were used as described in Ko16 (see also Table 1). Of those 16 stations 7 are already included in
10 the step 1 inversion. All provided valid values were used, except those paired flask
11 measurements that differ more than 0.34 ppm which were omitted. Measurements from the
12 continuous stations were aggregated to hourly values where needed, and neighboring values
13 differing by more than 1 ppm were omitted. Night and day time observations were selected
14 depending on the type of station (Ko16). As all institutions report mixing ratio values traceable
15 to WMO (World Meteorological Organization) calibration scale, we expect compatibility
16 between the different datasets (also see Rödenbeck et al., 2006).

17 In this study we use the site HEI (Heidelberg) which is traditionally not used for European CO₂
18 flux inversions as being considered too local (Broquet et al., 2013; Rödenbeck et al., 2009;
19 Rivier et al., 2010). The Heidelberg region is considered to be one of the most polluted regions in
20 Germany (Fiedler et al. 2005) and therefore could bias the flux estimates. Moreover the WES
21 (Westerland) site contains long periods with no data. This could potentially affect posterior flux
22 estimates since extended data gaps can lead to jumps in the presence of biases. Thus we evaluate
23 the performance and the sensitivity of the European flux estimates to the network configuration,
24 by performing also an inversion (referred to as S2, see Table 2) excluding HEI and WES.

25

26



1 **2.3 A-priori information and uncertainties**

2

3 A set of inversion cases differing in the prior information, the error structure and the station
4 configuration was realized (see overview in Table 2). Prior information derived from both
5 biosphere models (VPRM and GBIOME-BGCv1) is used to investigate the impact of the prior
6 fields to the posterior flux estimates. Furthermore an ensemble of inversions using different error
7 structures is used to investigate the impact on the posterior flux estimates and uncertainties.

8 Similarly to the synthetic inversion (Ko16) we use the base case B1 which inflates the prior
9 uncertainty by up-scaling the error covariance matrix, and case S1 which includes a bias term. In
10 the base case the VPRM model provides the prior flux field, and exponentially decaying
11 correlations are assumed. The bias component in the S1 scenario will always have a correction
12 with the same sign for all grid-cells as it just scales a predefined flux field. In the S1 case it
13 follows the shape of the annually averaged respiration flux, in the S1a case that of the a priori net
14 biogenic flux, and in the S1b case again that of the annually averaged respiration flux, but with
15 monthly temporal resolution of the bias term to allow for some temporal flexibility. The B2
16 inversion refers to the scenario where GBIOME-BGCv1 was used as a priori information instead
17 of VPRM, and the error structure does not contain a bias term. With this case we can evaluate
18 how sensitive the posterior flux estimates are with respect to the prior information which has
19 been used. We also examine a spatial error structure based on a hyperbolic (instead of an
20 exponential) spatial correlation shape as suggested in Chevallier et al. (2012) which we will refer
21 to as S3 scenario.

22 Note that in most of the inversions performed, VPRM fluxes were used as prior information.
23 Those fluxes are already optimized using EC measurements, therefore evaluation of the posterior
24 flux estimates against EC data at the local scale could result in posterior fluxes that are limited or
25 even not further constrained (since they are already optimized). In contrast, posterior fluxes
26 produced with BIOME-BGC used as prior are expected to show significantly larger corrections
27 compared to the prior estimations, and are therefore used for evaluation against EC data.
28 Nevertheless in most cases we use VPRM as prior in order to keep our estimates as data-driven



1 as possible through the overall optimization procedure; at local scale by using EC data, and at
2 regional scale using the atmospheric dry mole fractions.

3 As in the synthetic experiment (Ko16) the temporal decorrelation time was set to 31 days. In
4 Kountouris et al. (2015), model-data comparisons representative at site scale (around 1 km)
5 showed spatial correlation lengths of 40 km whilst model-model comparisons representative at
6 50 km resolution identified a correlation scale of 370 km. Considering also that the state space
7 has a resolution of 50 km, the spatial decorrelation length was chosen to be approximately 100
8 km (66 km in meridional, and 130 km in zonal direction). In the prior error covariance, diagonal
9 elements of $2.27 \mu\text{molm}^{-2}\text{s}^{-1}$ were assumed, consistent with the model-data flux mismatches as
10 calculated in Kountouris et al. (2015). Propagating this spatiotemporal error structure yields a
11 domain-integrated uncertainty (E_{st}) of 0.15 GtC y^{-1} . Note that this is substantially smaller than
12 for the synthetic experiment due to the much shorter spatial correlation length scales. A total
13 annual, domain integrated uncertainty E_{tot} of 0.3 GtC y^{-1} was assumed, which corresponds to
14 twice the standard deviation of annual terrestrial flux estimates for 2007 between terrestrial
15 biosphere models taken from the global carbon atlas (<http://www.globalcarbonatlas.org>). This is
16 also consistent with the prior uncertainty (for Europe) assumed for the global inversions
17 performed by the Jena inversion system. For those inversions in which the additional bias term
18 was considered (S1, S1a, and S1b scenarios), its error E_{BT} was calculated using

$$19 \quad E_{tot}^2 = E_{ST}^2 + E_{BT}^2 \quad (2)$$

20 For the S3 scenario using hyperbolic correlations similar to Chevallier et al. (2012) ($\frac{1}{1+d}$), a
21 characteristic value d (lag distance) was used such that the correlation drops after around 60 km
22 to $1/e$ of its initial value, consistent with the hyperbolic fit to the model-data flux residual
23 autocorrelation in Kountouris et al. (2015). For this case no additional bias term was needed, as
24 the spatially and temporally aggregated uncertainty was found to be 0.32 GtC y^{-1} , which is very
25 close to the uncertainty assumed for the inversions (0.3 GtC y^{-1}).

26 Furthermore, we include ocean fluxes from Mikaloff-Fletcher et al. (2007), and anthropogenic
27 emissions from the EDGAR v4.1 inventory scaled at national level for individual years
28 according to the BP (British Petroleum) statistical review of world energy (BP, 2012) following



1 Steinbach et al. (2011). Anthropogenic emissions are considered to be perfectly known (with no
2 prior uncertainty), as one typically assumes that there is more a-priori knowledge regarding the
3 anthropogenic emissions as compared to biogenic fluxes. As the inversion cannot distinguish
4 between biogenic and anthropogenic signals, any errors in the a-priori anthropogenic emissions
5 will be included as corrections to the NEE flux.

6

7 **2.4 Diagnostics and aggregation of fluxes**

8

9 Similar to Ko16 we use the χ_c^2 metric to evaluate the goodness of fit for each station (Eq. 3)

$$10 \quad \chi_c^2 = \frac{\sum_t \frac{(\Delta c_t)^2}{\sigma_t^2}}{n} \quad (3)$$

11 where Δc_t is the model-data mismatch in dry mole fractions for a given observation time t , n the
12 number of observations and σ_t the assumed uncertainty. Further we make use also of the reduced
13 χ_r^2 (Eq. 4) where J_{min} is the cost function at its minimum

$$14 \quad \chi_r^2 = 2 \frac{J_{min}}{n} \quad (4)$$

15 For more details about the chi-square metric the reader is referred to Ko16 study.

16 The optimized fluxes are derived at 0.25° spatial and daily temporal resolution from the inversion
17 system. We post-process the fluxes by aggregating them spatially at country/domain-wide scales
18 and temporally at monthly/annual scales.

19 Flux comparisons with other studies require that both fluxes refer to the same geographical
20 region. Typically studies refer to TransCom regions with a European domain that expands more
21 into the Eurasian region. To scale our results to the TransCom EU region, we calculated the flux
22 ratio between the TransCom EU region and our European domain from the first step of the two-
23 step inversion (global inversion), and used this ratio (about 1.3) to scale our posterior estimates
24 and the corresponding uncertainties (presented in Fig. 7).



1 **3 Results**

2

3 **3.1 Simulated CO₂ and goodness of fit**

4

5 Figure 1 presents a comparison of observed and modeled daily averages of the nighttime (hours
6 23, 00, 1, 2, 3, 4 UTC) CO₂ dry air mole fractions for the Schauinsland station (SCH), a
7 mountain station, for the year 2007. The prior estimates (gray line) as derived from a forward
8 model run using VPRM flux fields are systematically lower than the observations (black line)
9 with the most divergent values occurring during the growing season. A similar pattern was found
10 for the other atmospheric stations. Posterior CO₂ timeseries from all the inversions are in much
11 closer agreement with the observations.

12 Table 3 summarizes the statistics between the modeled and the observed CO₂ dry mole fractions
13 for all stations based on daily averages using the respective sampling times for mountain and
14 other stations. Of note is that the real data inversions include errors due to the modeling of
15 transport, which is not the case in the synthetic experiment in Ko16 as the same transport model
16 was used for forward and inversion runs. Standard deviations of the posterior residuals (observed
17 – modeled) show an average decrease for all inversion setups and for all stations of 59%
18 compared to the prior residuals. Correlations between prior and observed as well as posterior and
19 observed mole fractions (also Table 3) were likewise increased on average from 0.48 to 0.93. Of
20 note is that B1 and B2, which use an inflated prior error covariance for the spatiotemporal
21 component, show larger improvement relative to the prior in RMSD and some limited
22 improvement in correlation coefficient, compared to those inversions where a bias component
23 was included (S1, S1a, S1b). Figure 2 visually summarizes the goodness of fit in a Taylor
24 diagram for cases B1 and S1, presenting prior and posterior estimates of the correlation and the
25 normalized standard deviation between modeled and observed CO₂ dry mole fraction time-series.
26 It is obvious that the additional flexibility of B1 in the spatiotemporal flux distribution results in
27 a better reproduction of the concentration variability. The same picture emerges when comparing
28 the B1 and B2 inversions to S3 (see Table 3). Although all these cases assume no explicit bias
29 term in the error structure, the larger correlations from areas farther away for the S3 case with a
30 hyperbolic correlation causes a reduced number of effective degrees of freedom, which results in



1 larger residuals in posterior-observed mole fractions (Table 3) comparable to those of the S1
2 case.

3 Calculating the goodness of fit using the station-specific χ_c^2 values from Eq. (3), most of the sites
4 (Table 3) show values around 1, indicating that the misfits are inside the uncertainty range. For
5 the CBW, HEI, JFJ, KAS sites, values above 1 regardless the error structure were found, with the
6 most extreme value of 5.17 for the HEI site in the S3 inversion. This could suggest that for a
7 polluted site as HEI larger uncertainties should be considered.

8 The reduced χ_r^2 values regarding the overall model performance (Eq. 4) for all inversion set ups
9 is found to be close to 1 with χ^2 values of 1.08 (B1), 1.16 (B2), 1.17 (S1), 1.17 (S1a), 1.19 (S1b),
10 0.89 (S2) and 1.25 (S3), suggesting that the assumed prior uncertainty describes well the actual
11 uncertainties.

12

13 **3.2 Posterior flux estimates at different scales**

14

15 The annually integrated spatial flux distribution is presented in Fig. 3 for all the different
16 inversion settings. Differences between the results based on the two general error structures (with
17 and without the bias term) were observed mainly in central and Western Europe (longitudes less
18 than 20° E), where the network provides a strong constraint. This difference is characterized by
19 stronger spatial flux variability for the general B1 case, with multiple transitions between carbon
20 sources and sinks at regional scales. The same picture emerges for the western part of Europe. In
21 contrast, all the inversions including a bias component (S1, S1a, S1b) yield a more homogeneous
22 flux distribution with somewhat finer structure in the flux retrievals (e.g France and north-east
23 part of Europe). Comparisons between S1, S1a, S1b flux distributions do not show any
24 significant difference. Almost the same picture emerges when comparing B1 and S2 cases,
25 indicating that excluding the 2 stations does not have a very strong influence on our annual flux
26 estimates. However spatial differences were observed for the areas close to the two sites. The
27 most important one applies for the area near the HEI station where we observed a transition from
28 source to net carbon sink when excluding the corresponding site. The choice of the prior does
29 only have a small impact on the mean flux as can be seen by comparing posterior fluxes from B1



1 and B2 despite the significant differences in the flux innovations (Fig. 3). All innovations show
2 that positive fluxes were added mainly in central Europe and more intensively for the cases where
3 no bias term was used. Overall the results suggest that the general error structure matters, i.e.
4 whether or not to include a bias term, but how the bias is implemented is of less importance for
5 the retrieved flux patterns. One would expect that the flux distribution from the S3 case would
6 follow the general flux structure from the inversions without the bias term. Interestingly the
7 distribution is similar to the one obtained from the inversions with the bias term (cases S1, S1a,
8 and S1b). This shows that inversions assuming correlations with a strong contribution from the
9 far field have similar characteristics as inversions that assume a flat bias term.

10 Figure 4 shows the spatially aggregated posterior flux estimates for the full domain with the
11 corresponding uncertainties integrated at monthly and at annual temporal scales. The same prior
12 uncertainty was used for cases B1 and B2 although they differ in prior flux field. Posterior
13 estimates from B1 (blue line/shading) and B2 (green line/shading) inversions do not show any
14 significant difference at monthly and annual scales despite the large difference in prior fluxes.
15 We observe that the maximum uptake occurs slightly earlier for the B2 case. Monthly fluxes
16 from the S3 inversion also show the same temporal evolution. We do not observe any significant
17 difference in monthly fluxes for the S1 (red line/shading) and S1a (violet line/shading)
18 inversions. Both cases are comparable to the B1 and B2 cases at monthly and annual scales. A
19 slightly different picture emerges from the S1b inversion, where the bias term allowed for more
20 degrees of freedom for monthly corrections. The resulting seasonal cycle is somewhat smaller,
21 with reduced summer carbon uptake. Inversions that included the bias term yielded smaller
22 posterior uncertainties at both temporal scales, which is expected as the spatiotemporal
23 component of the uncertainty was not inflated as was the case for the B1 scenario. Flux retrievals
24 from the reduced network (sensitivity case S2) show a slightly deeper sink, but the differences to
25 the base case B1 are insignificant (i.e. clearly within the posterior uncertainties).

26 All of the inversions suggest Europe to be a carbon sink, with a range of $-0.23 \pm 0.13 \text{ GtC y}^{-1}$ to -
27 $0.38 \pm 0.17 \text{ GtC y}^{-1}$ for the S1b and B1 inversions respectively. The mean annual posterior flux
28 estimate for Europe averaged over different inversions amounts to -0.32 GtC y^{-1} .

29 Posterior monthly flux estimates at smaller spatial scales (country level) are shown in Fig. 5.
30 Areas that are not well constrained by the current network show some divergence in the posterior



1 flux estimates although not significant considering the uncertainty range. For example Germany,
2 which is better constraint, shows a limited spread of the posterior fluxes with an annually
3 averaged standard deviation between the different posterior flux estimates being $0.0009 \text{ GtC y}^{-1}$,
4 while United Kingdom (which is less well constrained) shows a slightly larger spread of the
5 posterior estimates with an annually averaged standard deviation of 0.002 GtC y^{-1} . Note that the
6 posterior uncertainties are smaller by about 36% for the S1 case, which is related to the smaller
7 prior uncertainties at monthly time scales (see also section 3.2 in Ko16).

8

9 3.3 Validation against eddy covariance measurements

10

11 As shown in Ko16, eddy covariance measurements in principle have the potential for
12 quantitative evaluation of the retrieved fluxes from the inversions. Here we used posterior flux
13 estimates from the B2 inversion for evaluation against eddy covariance measurements, as the
14 prior flux fields in B2 (GBIOME-BGCv1) were not optimized using eddy covariance
15 measurements. Gap-filled data were downloaded from the European Fluxes Database Cluster
16 (<http://www.europe-fluxdata.eu>). A modified flux-site network compared to the one reported in
17 Kountouris et al. (2015) was used. Specifically we omitted sites that they have not been used for
18 the VPRM optimization (*CH-Fru*, *CH-Lae*, *CH-Oel*, *ES-LMa*, *FR-Avi*, *FR-Mau*, *IT-Cas*, *IT-*
19 *LMa*, *IT-Ro2*, *NL-Dij*, *NL-Lut*, *SE-Skl*, *SK-Tat*) as well as sites that were not available as gap-
20 filled data (*CH-Dav*, *ES-Agu*, *FR-Aur*). Further some more sites were added both for the VPRM
21 optimization and for the flux comparisons (*CZ-wet*, *DK-Sor*, *HU-Bug*, *IT-Non*, *NL-Ca1*, *PL-wet*,
22 *RU-Fyo*, *UK-PL3*). Monthly averaged fluxes were extracted, with weights for each vegetation
23 class that compensate for the asymmetry between number of flux towers per vegetation type and
24 the fraction of land area covered by the specific vegetation type, similar to Ko16.

25 The analysis of the monthly prior biospheric fluxes in Fig. 6 reveals significant differences
26 between observed and prior fluxes from the inversion. The GBIOME-BGCv1 model
27 systematically overestimates the observed fluxes throughout the year. The retrieved fluxes from
28 the inversion (dark green line) are closer to the observed fluxes, with a stronger uptake compared
29 to the prior during spring and summer time. The timing of the peak uptake is shifted to one



1 month earlier in comparison to the observations. The mean absolute bias (averaged absolute
2 differences between prior/posterior and observed fluxes) is significantly reduced by 52% from
3 0.84 to 0.40 $\text{gCm}^{-2}\text{day}^{-1}$. The standard deviation of the residuals is reduced by around 24%, from
4 0.68 for the prior to 0.40 $\text{gCm}^{-2}\text{day}^{-1}$ for the posterior residuals. Splitting the sites into two main
5 categories, the first only with crops, and the second with non crop sites, revealed differences on
6 how well those sites can be represented. Clearly best matches were found for the non crop sites
7 with a reduction in the mean absolute bias of 51% whilst for the crop sites it is limited to 38%.

8

9 **4 Discussion**

10

11 We performed a series of atmospheric CO_2 inversions based on atmospheric data taken from 16
12 European stations for 2007. Different data-driven error structures in the prior error covariance
13 were assessed, and optimized biospheric fluxes were retrieved and post-processed at various
14 temporal and spatial scales for further evaluation. In this part we discuss the fitting performance
15 of the inversion system, and we detail the comparisons between our flux estimates at grid,
16 national and continental scales against eddy covariance data and reported flux estimates from
17 previous studies. Finally we discuss how sensitive flux retrievals are in the presence of erroneous
18 representation of the fossil fuel fluxes, and the site selection.

19

20 **4.1 Goodness of fit**

21

22 Site-specific misfits show a reasonable fit to the atmospheric data. Nevertheless in 4 cases
23 (CBW, HEI, JFJ, and KAS) site-specific χ_c^2 values were found to be larger than 1 (see also Table
24 3), indicating that either the model-data mismatch errors were chosen too small, or the
25 spatiotemporal resolution of the flux model is too coarse compared to the biosphere fluxes and
26 therefore small scale variations are not resolved (Rödenbeck et al., 2003). In fact this seems to be
27 the case for the JFJ and KAS sites as those are high altitude sites with steep cliffs. In such a
28 complex terrain the atmospheric circulation is hard to be simulated from the transport models.



1 Regarding CBW and in particular HEI, those are polluted sites and it would be reasonable to
2 assume larger model-data mismatch uncertainty since the model is too coarse to resolve the fossil
3 fuel emission patterns. One could argue that using higher spatial resolution to couple fossil fuel
4 fluxes with transport models might reduce the model-data mismatch uncertainties, and hence
5 improve posterior fluxes. To investigate that, we performed a forward run at coarser (0.25°) and
6 higher (1/12° lat. X 1/8° lon.) spatial resolution using only the fossil fuel emissions. As we use a
7 Lagrangian transport model, fluxes at higher resolution than that of the meteorological fields can
8 be used such that the simulated fossil fuel signals contain more spatially detailed information
9 (Lin et al., 2003). The derived concentration signal was subtracted from the observations and
10 subsequently an atmospheric inversion was performed. We report no significant differences
11 between the retrieved fluxes indicating that simply increasing the spatial resolution to about 10
12 km is not enough to correctly represent the fossil fuel distribution.

13 The reduced χ_r^2 values in our study (between 1.08 and 1.25) are larger than those found by Tolk
14 et al. (2011) where values between 0.34 and 0.78 were found for their pixel based inversion,
15 indicating a more conservative choice for their model-data mismatch errors. Even lower values
16 were reported in the study by Peylin et al. (2005) with values ranging from 0.01 up to 0.6
17 depending on the assumed correlations. χ^2 values from Zhang et al. (2015) were within a range of
18 1 to 4, but were modified by inflating the error covariances through an iterative procedure,
19 resulting in χ_r^2 values comparable to ours. Concluding, the χ_r^2 values give confidence that the
20 assumed prior uncertainties are well defined. We note though that examining the χ_r^2 values is not
21 always a sufficient metric to evaluate the defined uncertainties (Michalak et al., 2005; Chevallier,
22 2007).

23

24 **4.2 Validation against eddy flux measurements**

25

26 At the local scale the inversion shows ability to capture the observed flux variability at monthly
27 scale, as shown for the B2 case (see Fig. 6). The residuals between posterior model and eddy
28 covariance flux-data for monthly and site averaged fluxes show a range of misfits not exceeding
29 1.04 gCm⁻²day⁻¹ which is comparable with Broquet et al. (2013), where misfits up to



1 1.5 $\text{gCm}^{-2}\text{day}^{-1}$ were found using 6 years of data (2002-2007). Of note is that the estimated
2 carbon uptake agrees well with the estimated uptake for 2007 in Broquet et al. (2013) (within the
3 uncertainty range). However, in contrast to the synthetic inversion, the real data inversion
4 showed a larger monthly averaged posterior bias equal to $0.40 \text{ gCm}^{-2}\text{day}^{-1}$ compared to the -0.04
5 $\text{gCm}^{-2}\text{day}^{-1}$ for the synthetic case in Ko16. The poorer performance in terms of bias compared to
6 the synthetic case is presumably mainly caused by the representation error. In the synthetic
7 inversion we created a true flux field at the same spatial resolution as the posterior flux
8 estimates, and sampled this true flux distribution at the specific eddy covariance measurement
9 location. This does not include any spatial representation error of the EC measurements
10 (footprint about 1 km) with respect to the spatial resolution of 25 km at which the fluxes are used
11 within the inversion. A further cause for this poorer performance is related to the transport error,
12 as in the synthetic case the same transport was used to create the synthetic observations and to
13 perform the inversion, while in the real data inversions the observed atmospheric mole fraction
14 are a result of real transport which can only be approximated with the transport model used for
15 the inversion.

16 Differences between posterior flux retrievals and observed NEE fluxes at the eddy covariance
17 stations are clearly driven from the crop sites. The good agreement between posterior inverse
18 flux estimates and fluxes measured with the eddy covariance technique at non-crop sites can be
19 attributed to the relatively stable, within the year, land condition. Contrastingly, crop areas are
20 subject to human activities throughout the year. Soil enrichment with organic fertilizers,
21 irrigation and harvesting, can severely influence the carbon balance of the local ecosystem. Thus
22 the poor performance between inverse estimates and eddy covariance flux measurements at crop
23 sites can be linked to the extensive anthropogenic influence on those areas. Further it is worth to
24 mention that atmospheric concentrations implicitly contain more components than just the NEE
25 signal e.g. fire emissions. Such emissions are captured in the atmospheric observations
26 (representative scale of hundreds of km) but might not be captured from the eddy covariance flux
27 measurements which they have a very short representative scale of around 1 km.

28



1 4.3 Reliability of European flux estimates

2 4.3.1 Mismatch in bottom-up and top-down methods

3

4 Of note is the strong flux correction when using a-priori fluxes from VPRM with an uptake of
5 0.96 GtC y^{-1} compared to the 0.3 GtC y^{-1} after the inversion. The large correction of about 0.66
6 GtC y^{-1} corresponds to roughly twice the prior uncertainty. We note that VPRM is a diagnostic
7 model which uses simple light use efficiency and respiration equations and MODIS indices, with
8 parameters optimized to match hourly observations of NEE fluxes (Mahadevan et al., 2008). It
9 does not account for land management and land use changes (i.e. crop harvest, deforestation),
10 thus it will estimate a strong sink even for lands that have been harvested, with the respiration
11 fluxes resulting from the use of the harvest (e.g. as food) not included. Those so-called lateral
12 carbon fluxes, that are seen by the atmospheric inversion, account for approximately 0.165 GtC
13 y^{-1} of the prior-posterior flux difference (Ciais et al., 2008). The rest of the difference of about
14 0.5 GtC y^{-1} might be related to local characteristics of eddy covariance sites, which VPRM is not
15 able to represent. Spatial variations of NEE from VPRM are driven by those of EVI, which is
16 used at a spatial resolution of 1 km. For example, a crop field with typical dimensions of 100 m –
17 200 m surrounded by other fields with different crop rotation (and differing phenology) are hard
18 to represent with 1 km resolution EVI (even with the highest possible resolution of 250 m for
19 MODIS reflectances). To quantitatively assess the impact of this representation error in
20 combination with the selection of sites used for the VPRM optimization, the annual domain wide
21 C-budget from VPRM was recalculated after omitting one site per vegetation type at a time and
22 optimizing the VPRM parameters (Jackknife delete-1 method). Detailed results are shown in
23 Table 4. The derived Jackknife standard error amounted to 0.54 GtC y^{-1} , with a dominant
24 contribution from the cropland vegetation class (0.50 GtC y^{-1}). This uncertainty can fully explain
25 the mismatch between the a priori and the posterior fluxes, and it emphasizes the importance of
26 site selection and site representativeness in up-scaling local eddy covariance measurements to
27 larger regions.

28 The estimated uncertainty for VPRM fluxes based on jackknifing is larger than the prior
29 uncertainties assumed for the atmospheric inversions. Hence, one could argue that the prior
30 fluxes using VPRM (which indicate a too strong sink) combined with a too small prior



1 uncertainty in the inversion leads to erroneous posterior flux estimates. However the optimized
2 biogenic fluxes from all inversions converge at the annual and domain-integrated scale. A
3 particular example is that of the B2 inversion. Even though the GBIOME-BGCv1 fluxes differ
4 greatly from those produced by VPRM, this inversion is fully in line with the results from the
5 rest of the inversions, indicating that the optimized flux estimates are not biased by the a priori
6 flux fields but instead are driven by the atmospheric data.

7 **4.3.2 Sensitivity to anthropogenic emissions**

8

9 Another source of biospheric flux misrepresentation is the fossil fuel inventories. As mentioned
10 in section 2.3 we do not allow for corrections in anthropogenic emissions, as they are assumed to
11 be better known than the terrestrial fluxes. An overestimation/underestimation in anthropogenic
12 emissions will thus lead to a stronger/weaker biospheric sink in atmospheric inversions. The
13 anthropogenic emissions we use are 0.32 GtCy^{-1} (27%) lower for the EU-12 countries compared
14 to those used by Rivier et al. (2010) (1.2 GtCy^{-1}). Peylin et al. (2011) estimates the difference
15 between national totals for the different emission inventories to be around 10%. In a study by
16 Ciais et al. (2009) uncertainties of total fossil-fuel CO_2 emissions in the European Union 25
17 member states were estimated to 19%, based on four different emission inventories. For the EU-
18 25 countries, EDGAR emissions were found to be 12% larger than the mean of the GAINS
19 (Greenhouse Gas and Air Pollution Interactions and Synergies), UNFCC (United Nations
20 Framework Convention on Climate Change) and CDIAC (Carbon Dioxide Information Analysis
21 Center) inventories (Ciais et al. 2009, table 2). Sensitivity tests with increased prior fossil fuel
22 emissions showed that the added fossil fuel increases the estimated uptake by almost 50%
23 relative to the added anthropogenic emissions. Taking an extreme scenario where the fossil fuel
24 emissions are increased by 17% or 0.3 GtC y^{-1} (resulting in 1.77 GtC y^{-1} compared to 1.47 GtC
25 y^{-1} total emissions for EU-domain), we estimate a European carbon sink for the B1 set up of -
26 $0.51 \pm 0.17 \text{ GtCy}^{-1}$ compared to $-0.38 \pm 0.17 \text{ GtC y}^{-1}$ for the standard B1 case. Thus the
27 additional assumed fossil fuel emissions increased the estimated uptake by 0.13 GtCy^{-1} , which is
28 about 44% of the added anthropogenic emissions. The fact that the resulting increase in the
29 biospheric sink does not fully correspond to the increase in assumed emissions is likely a result



1 of the sparse network, where emissions from regions further away from the measurement sites
2 are not fully registered in the simulated mole fractions.

3

4 **4.3.3 Sensitivity to site selection**

5

6 Uncertainties in vertical mixing and especially in the nocturnal boundary layer (Gerbig et al.,
7 2008) should be carefully addressed as they might lead to erroneous estimations of the carbon
8 uptake. Typically in atmospheric inversions the model-data mismatch error (measurement error
9 covariance) accounts also for uncertainties due to the transport (i.e. wrong representation of the
10 nocturnal boundary layer). The set of network stations includes 6 mountain stations, for which
11 we use night-time observations (day-time for non mountain stations) as these measurements are
12 considered to be representative for the free troposphere. Errors can be introduced if the
13 measurement height assumed in the transport model is within the modeled nocturnal stable
14 boundary layer while in the real world it is not, which would lead to an overestimation in the
15 simulated CO₂ signals from respiration or vice versa. In the inversion this would be compensated
16 by introducing stronger uptake fluxes to match the observed CO₂ time series. In order to
17 investigate whether our results are influenced by the use of mountain stations, we performed an
18 additional inversion using the B1 error structure, but excluding all these stations. The resulting
19 sink in Europe was found to be $-0.41 \pm 0.17 \text{ GtCy}^{-1}$ which is fully in line with B1 inversion using
20 all sites, suggesting that our estimates are not biased due to misrepresentation of the mountain
21 stations.

22

23 **4.3.4 Retrieved fluxes and comparison to previous inverse estimates**

24

25 The retrieved spatially resolved fluxes showed a sensitivity in their spatial patterns to the a priori
26 error structure, specifically to the inclusion of a bias component, as indicated by differences
27 between the B1 and S1 cases. Such differences were not identified in the synthetic experiment in
28 Ko16, however there a much larger spatial correlation length scale was assumed. In the synthetic
29 inversions the long correlation length (766 km at the zonal and 411 km at the meridional



1 direction) drastically reduces the effective number of degrees of freedom, forcing the fluxes to be
2 smoothly corrected, regardless of the use of the bias component. In the real data inversions the
3 shorter correlation length (around 100 km), combined with the required larger error inflation
4 (compared to the synthetic inversions) for the B1 and B2 cases, increases the effective number of
5 degrees of freedom. By using a bias component (S1, S1a, S1b cases) or by using the hyperbolic
6 correlation shape (S3) with stronger large-scale correlation, instead of inflating the
7 spatiotemporal error component, fluxes remain less flexible at gridscale.

8 Our knowledge regarding annual CO₂ flux estimates for Europe is still highly uncertain, in part
9 due to the limited number of regional inversions focusing on this domain. Flux estimates from
10 previous studies, mainly global inversions, show a wide range (Fig. 7). We estimated an annual
11 European carbon sink (ranging between -0.23 ± 0.13 and -0.38 ± 0.17 GtC y⁻¹ for the different
12 inversion scenarios, Fig. 4 d)), which is however representative for a smaller European region
13 compared to the TransCom European region typically used in other studies. The up-scaled flux
14 estimates (see also section 2.4) for the TransCom EU region have a range of -0.30 to -0.49 GtC
15 y⁻¹. Ciais et al. (2000) estimated a European sink of -0.3 ± 0.8 GtC y⁻¹ for the target period 1985-
16 1995, however in contrast to our study they used a global system and a gap filling algorithm
17 since 42% of the observational data were missing. A recent study from Peylin et al. (2013)
18 computed the mean European sink for the period 1998-2001 to be -0.44 ± 0.45 GtC y⁻¹ by
19 utilizing eleven different global inversion systems. Gurney et al. (2004) performed also global
20 inversions and found the mean European annual fluxes for 1992 – 1996 period to be -0.98 ± 0.4
21 GtC y⁻¹ which is larger compared to our estimations. Moreover, our results for the mean net
22 monthly fluxes over Europe agreed very well with Rivier et al. (2010) who estimated for the
23 1998-2001 time frame using five different transport models in their inversion that the maximum
24 seasonal uptake occurs in July and lies between -10 and -80 gCm⁻²month⁻¹, while our results
25 show maximum uptake in June with a range of -33 to -37 gCm⁻²month⁻¹ for the different
26 inversion cases. We note that the annual flux differences between our flux estimates and those
27 from other studies may be also caused due to the interannual flux variability. Nevertheless this
28 should not be expected to critically drive those differences since posterior uncertainties found to
29 be larger than interannual variations (Broquet et al., 2013) making the significance of the
30 variations questionable.



1 A recent study from Reuter et al. (2014) based on inversions using satellite observations
2 estimated the carbon budget for the TransCom European region. For the year 2007 the sink was
3 found to be $-1.1 \pm 0.30 \text{ GtC y}^{-1}$, much larger compared to most of other inversion estimates using
4 ground observations. However Feng et al. (2016) tried to investigate why atmospheric inversions
5 using satellite observations, show an elevated European uptake, through a series of sensitivity
6 tests. They linked the increased uptake when using satellite measurements to potential
7 observation biases and to the emission spatial patterns. Further Feng et al. (2016) highlighted that
8 the large European uptake is related up to 60-90 % from systematically higher modeled CO_2
9 fluxes transported into Europe from regions outside of the domain. As this looks to be a problem
10 related with column measurements this is not the case in our study since ground observations
11 were used. In addition we use the two step inversion scheme which limits the influence from the
12 far field as we calculate the concentration signal from outside the domain and subtract that from
13 the observations. Whilst the flux uncertainties outside the domain are not propagated, still they
14 can be expressed as uncertainties in the observation space. However if biases introduced from
15 the global inversion to the fluxes outside of the domain, then regional flux estimations may
16 differ.

17 At national scale we can compare our results to those obtained by Meesters et al. (2012) for the
18 Netherlands, who estimated the annual national carbon sink to about $-0.017 \pm 0.004 \text{ GtCy}^{-1}$. Our
19 estimations are very close, with a range of $-0.012 \pm 0.004 \text{ GtCy}^{-1}$ (S1 inversion) to $-0.014 \pm$
20 0.005 for the B2 inversion. Of note is that the carbon budget estimates for Netherlands agree
21 remarkably well despite the substantial differences between the two studies: Meesters et al.
22 (2012) used an inversion scheme that solves for scaling factors of the gross prior fluxes. Spatial
23 correlations of 100 km were assumed but only for photosynthetic fluxes within the same land use
24 class. In addition the domain of interest (Netherlands) has a stronger constraint as four stations
25 located within the domain were used, while our inversion only uses one station (CBW), with the
26 rest of the stations being at least 360 km away (WES). Both studies assume approximately the
27 same fossil fuel emissions (0.051 GtC y^{-1} vs. 0.053 GtC y^{-1} in Meesters et al. (2012)).

28 **5 Conclusions**

29



1 This study is a follow up work from Kountouris et al. (2016). In this second part, the inverse
2 modeling framework was deployed using real atmospheric data from 16 stations in Europe, to
3 infer biospheric carbon fluxes. Different prior error structures were assumed to investigate how
4 sensitive posterior fluxes are. The results are validated and compared at different temporal and
5 spatial scales. Satisfactory agreement was found when posterior inverse flux estimates were
6 compared against eddy covariance observations at local scale, as well as against previous studies
7 at national and continental scales, which gives us confidence for our carbon flux estimations. We
8 calculated a sink for the European continent which amounts of $-0.23 \pm 0.13 \text{ GtC y}^{-1}$ to $-0.38 \pm$
9 0.17 GtC y^{-1} depending on the assumed prior error structure.

10 A special effort was also made to avoid potential biased flux estimations due to site selection (i.e.
11 heavily polluted sites, or sites that are within the nocturnal boundary layer) by performing
12 inversions using different network configurations. We did not observe any significant impact at
13 least for monthly and annual scales. Further we studied also how sensitive biospheric carbon
14 fluxes are, when wrong fossil fuel emissions are assumed. We found that due to the network
15 sparseness the fossil fuel emissions are not fully captured in the simulated mole fractions which
16 may bias the flux estimates.

17

18 **Acknowledgments**

19 This work contributed to the European Community's Seventh Framework Program (FP7) project
20 ICOS-INWIRE, funded under grant agreement no. 313169. The authors would also like to thank
21 the Deutsches Klimarechenzentrum (DKRZ) for using the high performance computing
22 facilities. The authors are also grateful to Max – Planck – Gesellschaft (MPG) for funding the
23 article fees and the high performance computing. The authors would like to thank all station PI's
24 for providing the data and in specific: A.T. Vermeulen, E. Dlugokencky, M. Galli, J.A. Morgui,
25 J. Necki, J.V. Lavric, M. Leuenberger, M. Ramonet, L. Haszpra, F. Meinhardt, M. Schumacher
26 and S. Hammer. This work used atmospheric CO₂ data acquired by the following sites, sorted by
27 project/funding agency: JFJ, HUN were funded by CarboEurope IP (GOCE-CT-2003-505572)
28 and IMECC (026188-I3), PRS is funded under Contract Agreement between RSE and the
29 Ministry of Economic Development-General Directorate for Nuclear Energy, Renewable Energy



1 and Energy Efficiency, CBW is funded by CarboEurope IP, CHIOTTO, and Min. of
2 Environment NLand BSIK ME02, OXK was funded by MPG, BIK was funded by MPG,
3 CHIOTTO (EVK2-CT-2002-00163) and CarboEurope IP (GOCE-CT-2003-505572), HEI was
4 funded by CarboEurope IP (GOCE-CT-2003-505572), MHD and PUY were coordinated by
5 LSCE (CEA/CNRS/UVSQ) as part of the SNO-RAMCES/ICOS monitoring network. This
6 publication is an outcome of the International Space Science Institute (ISSI) Working Group on
7 "Carbon Cycle Data Assimilation: How to consistently assimilate multiple data streams.

8

9

10

11

12 **References**

13 Alemanno, M., Di Diodato, A., Lauria, L. and Santobuono, N.: Environmental measurements at
14 Monte Cimone GAW station, *Int. J. Global Warming*, Vol. 6, No. 4, 424–454, doi:
15 10.1504/IJGW.2014.066048 2014.

16 Basu, S., Guerlet, S., Butz, A., Houweling, S., Hasekamp, O., Aben, I., Krummel, P., Steele,
17 P., Langenfelds, R., Torn, M., Biraud, S., Stephens, B., Andrews, A., and Worthy, D.:
18 Global CO₂ fluxes estimated from GOSAT retrievals of total column CO₂, *Atmos. Chem. Phys.*,
19 13, 8695–8717, doi:10.5194/acp-13-8695-2013, 2013.

20 BP (British Petroleum): Statistical Review of World Energy 2012: <http://www.bp.com/statisticalreview>, last access: December 2013, 2012.

22 Broquet, G., Chevallier, F., Bréon, F. M., Kadygrov, N., Alemanno, M., Apadula, F., Hammer,
23 S., Haszpra, L., Meinhardt, F., Morguá, J. A., Necki, J., Piacentino, S., Ramonet, M., Schmidt,
24 M., Thompson, R. L., Vermeulen, A. T., Yver, C., and Ciais, P.: Regional inversion of CO₂
25 ecosystem fluxes from atmospheric measurements: reliability of the uncertainty estimates,
26 *Atmos. Chem. Phys.*, 13, 9039-9056, doi:10.5194/acp-13-9039-2013, 2013.



- 1 Broquet, G., Chevallier, F., Rayner, P., Aulagnier, C., Pison, I., Ramonet, M., Schmidt, M.,
2 Vermeulen, A. T. and Ciais, P.: A European summertime CO₂ biogenic flux inversion at
3 mesoscale from continuous in situ mixing ratio measurements, *J Geophys. Res.*, 116, D23303,
4 doi:10.1029/2011JD016202, 2011.
- 5 Carouge, C., Bousquet, P., Peylin, P., Rayner, P. J., and Ciais, P.: What can we learn from
6 European continuous atmospheric CO₂ measurements to quantify regional fluxes – Part 1:
7 Potential of the 2001 network, *Atmos. Chem. Phys.*, 10, 3107-3117, doi:10.5194/acp-10-3107-
8 2010, 2010a.
- 9 Carouge, C., Peylin, P., Rayner, P. J., Bousquet, P., Chevallier, F., and Ciais, P.: What can we
10 learn from European continuous atmospheric CO₂ measurements to quantify regional fluxes –
11 Part 2: Sensitivity of flux accuracy to inverse setup, *Atmos. Chem. Phys.*, 10, 3119-3129,
12 doi:10.5194/acp-10-3119-2010, 2010b.
- 13 Chevallier, F., Wang T., Ciais P., Maignan F., Bocquet M., Altaf A. M., Cescatti A., Chen J.,
14 Dolman A., J., Law B. E., Margolis, H. A., Montagnani, L., Moors, E. J.: What eddy-covariance
15 measurements tell us about prior land flux errors in CO₂ flux inversion schemes, *Glob.*
16 *Biogeochem. Cy.*, 26, GB1021, doi:10.1029/2010GB003974, 2012.
- 17 Chevallier, F., Palmer, P. I., Feng, L., Bösch, H., O'Dell, C., and Bousquet, P.: Towards
18 robust and consistent regional CO₂ flux estimates from in situ and space-borne
19 measurements of atmospheric CO₂, *Geophys. Res. Lett.*, 41, 1065–1070,
20 doi:10.1002/2013GL058772, 2014.
- 21 Ciais, P., Peylin, P. and Bousquet, P.: Regional biospheric carbon fluxes as inferred from
22 atmospheric CO₂ measurements, *Ecol Appl*, 10, 1574-1589, doi: 10.2307/2641225, 2000.
- 23 Ciais, P., Borges, A. V., Abril, G., Meybeck, M., Folberth, G., Hausglustaine, D., and Janssens,
24 I. A.: The impact of lateral carbon fluxes on the European carbon balance, *Biogeosciences*, 5,
25 1259-1271, doi: 10.5194/bg-5-1259-2008, 2008.
- 26 Ciais, P., Paris, J. D., Marland, G., Peylin, P., Piao, S. L., Levins, I., Pregger, T., Scholz, Y.,
27 Friedrich, R., Rivier, L., Houwelling, S., Schulze, E. D., and members of the CARBOEUROPE



- 1 SYNTHESIS TEAM: The European carbon balance. Part1: fossil fuel emissions, *Glob Change*
2 *Biol*, 16, 1395-1408, doi: 10.1111/j.1365-2486.2009.02098.x, 2009.
- 3 Dee, D. P., Uppala, S. M., Simmons, A. J., Berrisford, P., Poli, P., Kobayashi, S., Andrae, U.,
4 Balmaseda, M. A., Balsamo, G., Bauer, P., Bechtold, P., Beljaars, A. C. M., van de Berg, L.,
5 Bidlot, J., Bormann, N., Delsol, C., Dragani, R., Fuentes, M., Geer, A. J., Haimberger, L., Healy,
6 S. B., Hersbach, H., Hólm, E. V., Isaksen, L., Kállberg, P., Köhler, M., Matricardi, M., McNally,
7 A. P., Monge-Sanz, B. M., Morcrette, J.-J., Park, B.-K., Peubey, C., de Rosnay, P., Tavolato, C.,
8 Thépaut, J. N. and Vitart, F.: The ERA-Interim reanalysis: configuration and performance of the
9 data assimilation system. *Q.J.R. Meteorol. Soc.*, 137: 553–597. doi: 10.1002/qj.828, 2011.
- 10 Deng, F., Jones, D. B. A., Henze, D. K., Bousserez, N., Bowman, K. W., Fisher, J. B., Nassar,
11 R., O'Dell, C., Wunch, D., Wennberg, P. O., Kort, E. A., Wofsy, S. C., Blumenstock, T.,
12 Deutscher, N. M., Griffith, D. W. T., Hase, F., Heikkinen, P., Sherlock, V., Strong, K.,
13 Sussmann, R., and Warneke, T.: Inferring regional sources and sinks of atmospheric CO₂
14 from GOSAT XCO₂ data, *Atmos. Chem. Phys.*, 14, 3703–3727, doi:10.5194/acp-14-3703-2014,
15 2014.
- 16 Dlugokencky, E.J., Lang, P.M., Masarie, K.A., Crotwell, A.M., and Crotwell, M. J.:
17 Atmospheric Carbon Dioxide Dry Air Mole Fractions from the NOAA ESRL Carbon Cycle
18 Cooperative Global Air Sampling Network, 1968-2014, Version: 2015-08-03, Path:
19 ftp://aftp.cmdl.noaa.gov/data/trace_gases/co2/flask/surface/.
- 20 Feng, L., Palmer, P. I., Parker, R. J., Deutscher, N. M., Feist, D. G., Kivi, R., Morino, I., and
21 Sussmann, R.: Estimates of European uptake of CO₂ inferred from GOSAT XCO₂ retrievals:
22 sensitivity to measurement bias inside and outside Europe, *Atmos. Chem. Phys.*, 16, 1289-1302,
23 doi: 10.5194/acp-16-1289-2016, 2016.
- 24 Ferrarese S., Apadula F., Bertiglia F., Cassardo C., Ferrero A., Fialdini L., Francone C., Heltai
25 D., Lanza A., Longhetto A., Manfrin M., Richiardone R., Vannini C.: Inspection of high-
26 concentration CO₂ events at the Plateau Rosa Alpine station, *Atmos. Pollution Res.*, 6, 3, 415-
27 427, doi:10.5094/APR.2015.046, 2015.
- 28 Fiedler, V., Dal Maso, M., Boy, M., Aufmhoff, H., Hoffmann, J., Schuck, T., Birmili, W.,
29 Hanke, M., Uecker, J., Arnold, F., and Kulmala, M.: The contribution of sulphuric acid to



- 1 atmospheric particle formation and growth: a comparison between boundary layers in Northern
2 and Central Europe, *Atmos. Chem. Phys.*, 5, 1773-1785, doi:10.5194/acp-5-1773-2005, 2005.
- 3 Gerbig, C., Körner, S. and Lin, J. C.: Vertical mixing in atmospheric tracer transport models:
4 error characterization and propagation, *Atmos. Chem. Phys.*, 8, 591-602, doi:10.5194/acp-8-591-
5 2008, 2008.
- 6 Gurney, K. R., Law, R. M., Denning, A. S., Rayner, P. J., Baker, D., Bousquet, P., Bruhwiler, L.,
7 Chen, Y.-H., Ciais, P., Fan, S., Fung, I. Y., Gloor, M., Heimann, M., Higuchi, K., John, J.,
8 Kowalczyk, E., Maki, T., Maksyutov, S., Peylin, P., Prather, M., Pak, B. C., Sarmiento, J.,
9 Taguchi, S., Takahashi, T., and Yuen, C. W.: TransCom and CO₂ inversion intercomparison 1.
10 Annual and mean control results and sensitivity to transport and prior flux information, *Tellus*
11 55B, 555-579, doi: 10.1034/j.1600-0889.2003.00049.x, 2003.
- 12 Gurney, K. R., Rachel M. L., Denning, A. S., Rayner, P. J., Bernard C. P., Baker, D., Bousquet,
13 P., Bruhwiler, L., Chen, Y.-H., Ciais, Fung, I. Y., Heimann, M., John, J., Maki, T., Maksyutov,
14 S., Peylin, P., Prather, M. and Taguchi, S.: Transcom 3 inversion intercomparison: Model mean
15 results for the estimation of seasonal carbon sources and sinks, *Global Biogeochem. Cy.*, 18,
16 GB1010, doi:10.1029/2003GB002111, 2004.
- 17 Hammer, S., Glatzel-Mattheier, H., Müller, L., Sabasch, M., Schmidt, M., Schmitt, S.,
18 Schönherr, C., Vogel, F., Worthy, D. E., and Levin, I.: A gas chromatographic system for high-
19 precision quasi-continuous atmospheric measurements of CO₂, CH₄, N₂O, SF₆, CO and H₂,
20 available at: "http://www.iup.uni-heidelberg.de/institut/forschung/groups/kk/GC_html" (last
21 access: 25 January 2016), 2008.
- 22 Haszpra, L., Barcza, Z., Bakwin, P.S., Berger, B.W., Davis, K.J., Weidinger, T.: Measuring
23 system for the long-term monitoring of biosphere/atmosphere exchange of carbon dioxide. *J.*
24 *Geophys Res*, 106D, 3057-3069, DOI: 10.1029/2000JD900600, 2001.
- 25 Heimann, M. and Körner, S.: The global atmospheric tracer model TM3, Tech. Rep. 5, MPI
26 BGC, Jena (Germany), online available at: [http://www.bgc-
27 jena.mpg.de/mpg/websiteBiogeochemie/Publikationen/Technical Reports/tech report5.pdf](http://www.bgc-jena.mpg.de/mpg/websiteBiogeochemie/Publikationen/Technical Reports/tech report5.pdf), 2003.



- 1 Houweling, S., Aben, I., Breon, F.-M., Chevallier, F., Deutscher, N., Engelen, R., Gerbig, C.,
2 Griffith, D., Hungershofer, K., Macatangay, R., Marshall, J., Notholt, J., Peters, W., and Serrar,
3 S.: The importance of transport model uncertainties for the estimation of CO₂ sources and sinks
4 using satellite measurements, *Atmos. Chem. Phys.*, 10, 9981-9992, doi:10.5194/acp-10-9981-
5 2010, 2010.
- 6 Kountouris, P., Gerbig, C., Totsche, K. U., Dolman, A. J., Meesters, A. G. C. A., Broquet, G.,
7 Maignan, F., Gioli, B., Montagnani, L., Helfter, C.: An objective prior error quantification for
8 regional atmospheric inverse applications, *Biogeosciences*, 12, 7403-7421, doi: 10.5194/bg-12-
9 7403-2015, 2015.
- 10 Kountouris, P., Gerbig, C., Rödenbeck, C., Karstens, U., Koch, F. Th., Heimann, M.:
11 Atmospheric CO₂ inversions at the mesoscale using data driven prior uncertainties. Part1:
12 Methodology and system evaluation, submitted in *Atmos. Chem. Phys.*, 2016.
- 13 Lin, J. C., Gerbig, C., Wofsy, S. C., Andrews, A. E., Daube, B. C., Davis, K. J., and Grainger, C.
14 A.: A near-field tool for simulating the upstream influence of atmospheric observations: The
15 Stochastic Time-Inverted Lagrangian Transport (STILT) model, *J. Geophys. Res.*, 108, 4493,
16 doi: 10.1029/2002JD003161, 2003.
- 17 Lin, J. C., and C. Gerbig: Accounting for the effect of transport errors on tracer inversions,
18 *Geophys. Res. Lett.*, 32, L01802, doi:10.1029/2004GL021127, 2005.
- 19 Lopez, M., Schmidt, M., Ramonet, M., Bonne, J. L., Colomb, A., Kazan, V., Laj, P., and Pichon,
20 J. M.: Three years of semicontinuous greenhouse gas measurements at the Puy de Dôme station
21 (central France), *Atmos. Meas. Tech.*, 8, 3941-3958, doi:10.5194/amt-8-3941-2015, 2015.
- 22 Mahadevan, P., Wofsy, S. C., Matross, D. M., Xiao, X., Dunn, A. L., Lin, J. C., Gerbig, C.,
23 Munger, J. W., Chow, V. Y. and Gottlieb, E. W.: A satellite-based biosphere parameterization
24 for net ecosystem CO₂ exchange: Vegetation Photosynthesis and Respiration Model (VPRM),
25 *Glob. Biogeochem. Cy.* 22, GB2005, doi: 10.1029/2006GB002735, 2008.
- 26 Meesters, A. G. C. A., Tolck, L. F., Peters, W., Hutjes, R. W. A., Vellinga, O. S., Elbers, J. A.,
27 Vermeulen, A. T., van der Laan, S., Neubert, R. E. M., Meijer, H. A. J., Dolman, A. J.: Inverse



- 1 carbon dioxide flux estimates for the Netherlands, *J. Geophys. Res.-Atmos.* 117, D20306, 1984-
2 2012, doi: 10.1029/2012jd017797, 2012.
- 3 Michalak, A., Hirsch, A., Bruhwiler, L., Gurney, K. R., Peters, W., and Tans, P. P.: Maximum
4 likelihood estimation of covariance parameters for Bayesian atmospheric trace gas surface flux
5 inversions, *J. Geophys. Res.*, 100, D24107, doi:10.1029/2005JD005970, 2005.
- 6 Mikaloff F., S. E., Gruber, N., Jacobson, A. R., Doney, S. C., Dutkiewicz, S., Gerber, M., Gloor,
7 M., Follows, M., Joos, F., Lindsay, K., Menemenlis, D., Mouchet, A., Müller, S. A., and
8 Sarmiento, J. L.: Inverse estimates of the oceanic sources and sinks of natural CO₂ and the
9 implied oceanic transport, *Glob. Biogeochem. Cy.*, 21, GB1010, doi:10.1029/2006GB002751,
10 2007.
- 11 Necki, J.M., Chmura, L., Zimnoch, M., Rozanski, K.: Impact of emissions on atmospheric
12 composition at Kasprowy Wierch based on results of carbon monoxide and carbon dioxide
13 monitoring, *Polish J. Environm. Studies*, 22, 4, 1119-1127, 2013.
- 14 Peters, W., Krol, M. C., van der Werf, G. R., Houweling, S., Jones, C. D., Hughes, J., Schaefer,
15 K., Masarie, K., Jacobson, A. R., Miller, J. B., Cho, C. H., Ramonet, M., Schmidt, M., Ciattaglia,
16 L., Apadula, F., Heltai, D., Meinhardt, F., DI Sarra, A. G., Piacentino, S., Sferlazzo, D., Aalto,
17 T., Hatakka, J., Stroem, J., Haszpra, L., Meijer, H. A. J., van der Laan, S., Neubert, R. E. M.,
18 Jordan, Rodo. X., Morgui, J. A., Vermeulen, A. T., Popa, E., Rozanski, K., Zimnoch, M.,
19 Manning, A. C., Leuenberger, M., Uglietti, C., Dolman, A. J., Ciais, P., Heimann, M., and Tans,
20 P.: Seven years of recent European net terrestrial carbon dioxide exchange constrained by
21 atmospheric observations, *Glob. Change Biol.*, 16, 1317-1337, doi: 10.1111/j.1365-
22 2486.2009.02078.x, 2010.
- 23 Peylin, P., Rayner, P., Bousquet, P., Carouge, C., Hourdin, F., Heinrich, P., Ciais, P. and
24 AEROCARB contributors: Daily CO₂ flux estimates over Europe from continuous atmospheric
25 measurements: 1, inverse methodology, *Atmos. Chem. Phys.* 5, 3173-3186, doi:10.5194/acp-5-
26 3173-2005, 2005.
- 27 Peylin, P., Houweling, S., Krol, M. C., Karstens, U., Rödenbeck, C., Geels, C., Vermeulen, A.,
28 Badawy, B., Aulagnier, C., Pregarer, T., Delage, F., Pieterse, G., Ciais, P., and Heimann, M.:



- 1 Importance of fossil fuel emission uncertainties over Europe for CO₂ modeling: model
2 intercomparison, *Atmos. Chem. Phys.*, 11, 6607-6622, doi:10.5194/acp-11-6607-2011, 2011.
- 3 Peylin, P., Law, R. M., Gurney, K. R., Chevallier, F., Jacobson, A. R., Maki, T., Niwa, Y., Patra,
4 P. K., Peters, W., Rayner, P. J., Rödenbeck, C., van der Laan-Luijkx, I. T., and Zhang, X.:
5 Global atmospheric carbon budget: results from an ensemble of atmospheric CO₂ inversions,
6 *Biogeosciences* 10, 6699-6720, doi: 10.5194/bg-10-6699-2013, 2013.
- 7 Popa, M. E., Gloor, M., Manning, A. C., Jordan, A., Schultz, U., Haensel, F., Seifert, T., and
8 Heimann, M.: Measurements of greenhouse gases and related tracers at Bialystok tall tower
9 station in Poland, *Atmos. Meas. Tech.*, 3, 407-427, doi:10.5194/amt-3-407-2010, 2010.
- 10 Ramonet, M., Ciais, P., Aalto, T., Aulagnier, C., Chevallier, F., Cipriano, D., Conway, T. J.,
11 Haszpra, L., Kazan, V., Meinardt, F., Paris, J. D., Schmidt, M., Simmonds, P., Xueref-Remy, I.
12 and Necki, J. N.: A recent build-up of atmospheric CO₂ over Europe. Part 1: observed signals
13 and possible explanations. *Tellus B*, 62: 1–13. doi: 10.1111/j.1600-0889.2009.00442.x, 2010
- 14 Reuter, M., Buchwitz, M., Hilker, M., Heymann, J., Schneising, O., Pillai, D., Bovensmann, H.,
15 Burrows, J. P., Bösch, H., Parker, R., Butz, A., Hasekamp, O., O'Dell, C. W., Yoshida, Y.,
16 Gerbig, C., Nehrkorn, T., Deutscher, N. M., Warneke, T., Notholt, J., Hase, F., Kivi, R.,
17 Sussmann, R., Machida, T., Matsueda, H., and Sawa, Y.: Satellite-inferred European carbon sink
18 larger than expected, *Atmos. Chem. Phys.*, 14, 13739-13753, doi:10.5194/acp-14-13739-2014,
19 2014.
- 20 Rivier, L., Peylin, P., Ciais, P., Gloor, M., Roedenbeck, C., Geels, C., Karstens, U., Bousquet, P.,
21 Brandt, J. and Heimann, M.: European CO₂ fluxes from atmospheric inversions using regional
22 and global transport models, *Climatic Change*, 103, 93-115, doi: 10.1007/s10584-010-9908-4,
23 2010.
- 24 Rödenbeck C., Houwelling S., Gloor M. and Heinmann, M.: CO₂ flux history 1982-2001
25 inferred from atmospheric data using a global inversion of atmospheric transport, *Atmos. Chem.*
26 *and Phys.* 3, 1919-1964, doi: 10.5194/acp-3-1919-2003, 2003.
- 27 Rödenbeck, C.: Estimating CO₂ sources and sinks from atmospheric mixing ratio measurements
28 using a global inversion of atmospheric transport, Technical Report 6, Max Planck Institute for



- 1 Biogeochemistry, Jena, <http://www.bgc-jena.mpg.de/mpg/websiteBiogeochemie/>
- 2 Publikationen/Technical Reports/tech report6.pdf, 2005.
- 3 Rödenbeck, C., Gerbig, C., Trusilova, K. and Heimann, M.: A two-step scheme for high-
- 4 resolution regional atmospheric trace gas inversions based on independent models, Atmos.
- 5 Chem. and Phys. 9, 5331-5342, doi:10.5194/acp-9-5331-2009, 2009.
- 6 Rödenbeck, C., Bakker, D. C. E., Metzl, N., Olsen, A., Sabine, C., Cassar, N., Reum, F.,
- 7 Keeling, R. F. and Heimann, M.: Interannual sea–air CO₂ flux variability from an observation-
- 8 driven ocean mixed-layer scheme, Biogeosciences, 11(17), 4599–4613, doi:10.5194/bg-11-4599-
- 9 2014-supplement, 2014.
- 10 Steinbach, J., Gerbig, C., Rödenbeck, C., Karstens, U., Minejima, C. and Mukai, H.: The CO₂
- 11 release and Oxygen uptake from Fossil Fuel Emission Estimate (COFFEE) dataset: effects from
- 12 varying oxidative ratios, Atmos. Chem. Phys., 11(14), 6855–6870, doi:10.5194/acp-11-6855-
- 13 2011, 2011.
- 14 Thompson, R. L., Manning, A. C., Gloor, E., Schultz, U., Seifert, T., Hänsel, F., Jordan, A., and
- 15 Heimann, M.: In-situ measurements of oxygen, carbon monoxide and greenhouse gases from
- 16 Ochsenkopf tall tower in Germany, Atmos. Meas. Tech., 2, 573-591, doi:10.5194/amt-2-573-
- 17 2009, 2009.
- 18 Tolk, L. F., Dolman, A. J., Meesters, A. G. C. A. and Peters, W.: A comparison of different
- 19 inverse carbon flux estimation approaches for application on a regional domain, Atmos. Chem.
- 20 Phys., 11, 10349-10365, doi: 10.5194/acp-11-10349-2011, 2011.
- 21 Trusilova, K., Rödenbeck, C., Gerbig, C., and Heimann, M.: Technical Note: A new coupled
- 22 system for global to regional downscaling of CO₂ concentration estimation, Atmos. Chem. Phys.
- 23 10, 3205-3213, doi:10.5194/acp-10-3205-2010, 2010.
- 24 Vermeulen, A. T., Hensen, A., Popa, M. E., Bulk, W. C. M., Jongejan, P. A. C.: Greenhouse gas
- 25 observations from Cabauw Tall Tower (1992-2010), Atmos. Meas. Tech., 4, 617-644,
- 26 doi:10.5194/amt-4-617-2011, 2011.



- 1 Zhang, S., Zheng, X., Chen, J. M., Chen, Z., Dan, B., Yi, X., Wang, L. and Wu, G.: A global
- 2 carbon assimilation system using a modified ensemble Kalman filter, Geoscientific. Model
- 3 Development., 8, 805-816, doi: 10.5194/gmd-8-805-2015, 2015.

4



1 Table 1. Information on the stations used for the regional inversions. Same network applied for
 2 the synthetic, and the real data inversions in Kountouris et al. (2016). In first column the term
 3 “type” stands for continuous (C) or flask (F) data. Under “Data origin” WDCGG means “World
 4 Data Centre for Greenhouse Gases”.

5

Site Code / type	Name	Latitude (°)	Longitude (°)	Height (m.a.s.l.) (m)	Measurement height (above ground) (m)	Model	Data provider	Data origin	Citation
BAL/F	Baltic Sea, Poland	55.50	16.67	8	57	28	NOAA	Direct contact	Dlugokency et al. 2015
BIK/C	Bialystok, Poland	53.23	23.03	183	90	90	MPI-BGC	Direct access	Popa et al. (2010)
CBW/C	Cabauw, Netherlands	51.58	4.55	-2	200	200	ECN	Direct contact	Vermeulen et al. (2011)
CMN/C	Monte Cimone, Italy	44.18	10.7	2165	12	670	IAFMS	WDCGG	Alemanno et al. (2014)
HEI/C	Heidelberg, Germany	49.42	8.67	116	30	30	University of Heidelberg	CarboEurope	Hammer et al. (2008)
HPB/F	Hohenpeissenberg, Germany	47.80	11.01	934	50	10	NOAA	Direct contact	-
HUN/C	Hegyhatsal, Hungary	46.95	16.65	248	115	96	HMS	WDCGG	Haszpra et al. (2001)
JFJ/C	Jungfraujoch, Switzerland	46.55	7.98	3572	10	720	University of Bern	CarboEurope	-
KAS/	Kasprowy	49.23	19.93	1987	5	480	UKRAK	CarboEurope	Necki et



C	Wierch								, AGH	ope	al. (2013)
LMU/ C	La Muela, Spain	41.36	-1.6	570	79	80	Universi ty of Barcelon a	CarboEur ope		-	
MHD/ C	Mace Head, Ireland	53.33	-9.90	25	10	15	LSCE	WDCGG		Ramonet et al. (2010)	
OXX/ C	Ochsenkopf, Germany	50.03	11.81	1022	163	163	MPI- BGC	CarboEur ope		Thompson et al. (2009)	
PRS/ C	Plateau Rosa, Italy	45.93	7.71	3480	-	500	RSE	WDCGG		Ferrarese et al. (2015)	
PUY/ C	Puy De Dome, France	45.77	2.97	1465	10	400	LSCE	CarboEur ope		Lopez et al. (2015)	
SCH/ C	Schauinsland, Germany	47.92	7.92	1205	-	230	UBA	WDCGG		-	
WES/ C	Westerland, Germany	54.93	8.32	12	-	15	UBA	WDCGG		-	

1 Glossary for the data providers: AGH: University of science and Technology Poland, ECN: Energy research Centre
 2 of the Netherlands, HMS: Hungarian Meteorological Service, IAFMS: Italian Air Force Meteorological Service,
 3 LSCE: Le Laboratoire des Sciences du Climat et de l'Environnement, MPI-BGC: Max Planck Institute for
 4 BioGeoChemistry, NOAA: National Oceanic and Atmospheric Administration, RSE: Ricerca sul Sistema
 5 Energetico, UBA: Umweltbundesamt, UKRAK: Department of Environmental Physics Poland

6

7

8



Table 2. Overview of the inversion scenarios. “Shape” describes the internal structure of the bias component (proportional to respiration R or to Net Ecosystem Exchange NEE), and “Time vary” indicates whether the bias component also has temporal variations or not. The fifth column “Prior” represents the terrestrial model used as prior, and “Correlation shape” describes the functional form used for the spatial prior uncertainty correlation, either exponential (E) or hyperbolic (H). The last column indicates whether the full or the reduced station network was assumed.

Inversion code	Bias component	Shape	Time vary	Prior	Correlation shape	No. of Stations
B1	-	-	-	VPRM	E	16
B2	-	-	-	GBIOME	E	16
S1	Yes	R	Flat	VPRM	E	16
S1a	Yes	NEE	Flat	VPRM	E	16
S1b	Yes	R	Vary	VPRM	E	16
S2	-	-	-	VPRM	E	14
S3	-	-	-	VPRM	H	16



Table 3. RMSD (first column in ppm) and correlation coefficients (second column) between observations and prior/posterior CO₂ dry mole fractions for daily “daytime” or “nighttime” averaged values and for each station. The third column shows χ_c^2 , the normalized dry mole fraction mismatch per degree of freedom for 7-day averaged residuals, as a measure of how well the data were fitted. The format for each station is as follows: RMSD | r² | χ^2 .

	Prior	B1	B2	S1	S1a	S1b	S2	S3
BAL	7.12 0.20 69.35	1.48 0.97 0.89	1.53 0.97 0.93	2.26 0.93 2.04	2.26 0.93 2.03	2.25 0.93 2.02	1.41 0.97 0.83	2.37 0.92 2.07
BIK	8.20 0.52 60.10	2.93 0.93 0.88	3.17 0.92 0.99	3.52 0.90 1.51	3.52 0.90 1.53	3.51 0.90 1.53	2.93 0.93 0.88	3.78 0.88 1.70
CBW	8.71 0.23 83.98	3.43 0.88 2.05	3.49 0.88 2.18	4.09 0.83 2.47	4.09 0.83 2.48	4.09 0.83 2.49	3.42 0.88 1.99	4.33 0.81 2.61
CMN	4.20 0.40 31.73	1.26 0.96 0.16	1.35 0.95 0.19	1.45 0.94 0.19	1.44 0.95 0.19	1.46 0.94 0.21	1.25 0.92 0.15	1.57 0.94 0.26
HEI	14.04 0.37 31.28	6.93 0.84 3.05	7.07 0.83 3.07	7.92 0.79 4.22	7.91 0.79 4.23	7.92 0.79 4.23	-	8.34 0.77 5.17
HPB	5.06 0.43 15.61	1.41 0.91 0.34	1.70 0.94 0.50	2.00 0.96 0.65	2.01 0.91 0.66	2.00 0.91 0.65	1.41 0.96 0.33	2.03 0.91 0.67
HUN	7.44 0.55 66.36	2.58 0.94 0.84	2.74 0.93 0.88	3.07 0.92 1.32	3.08 0.92 1.34	3.08 0.92 1.33	2.58 0.94 0.87	3.43 0.90 1.98
JFJ	4.52 0.03 21.39	1.96 0.77 1.59	2.23 0.72 1.53	2.07 0.75 1.83	2.07 0.75 1.82	2.07 0.75 1.84	1.95 0.78 1.58	2.10 0.74 1.98
KAS	6.35 0.39 52.58	3.41 0.87 2.90	3.43 0.87 2.89	3.88 0.82 3.96	3.88 0.82 3.99	3.87 0.83 3.93	3.29 0.77 2.77	4.01 0.81 4.67
LMU	6.01 0.05 29.00	1.45 0.94 0.29	1.51 0.94 0.28	1.74 0.92 0.59	1.74 0.92 0.58	1.76 0.92 0.60	1.44 0.95 0.29	1.84 0.91 0.68
MHD	4.50 0.21 22.24	1.23 0.94 0.24	1.20 0.94 0.21	1.29 0.92 0.31	1.74 0.93 0.31	1.76 0.94 0.31	1.23 0.94	1.26 0.94 0.27



							0.24	
OXK	5.39 0.28 38.95	2.45 0.85 0.79	2.52 0.84 0.85	2.78 0.81 1.19	2.78 0.81 1.20	2.79 0.81 1.20	2.41 0.86 0.70	2.98 0.78 1.59
PRS	2.98 0.07 20.75	1.06 0.89 0.46	1.10 0.88 0.49	1.16 0.87 0.52	1.16 0.87 0.52	1.17 0.87 0.52	1.07 0.89 0.45	1.22 0.86 0.53
PUY	4.86 0.29 39.48	2.05 0.87 0.67	2.16 0.86 0.75	2.40 0.82 0.97	2.40 0.82 0.97	2.40 0.82 0.95	2.02 0.88 0.71	2.48 0.81 1.27
SCH	5.18 0.24 41.77	1.90 0.89 0.27	2.00 0.88 0.28	2.23 0.85 0.51	2.23 0.85 0.51	2.23 0.85 0.51	1.84 0.90 0.24	2.38 0.84 0.70
WES	8.06 0.23 41.77	2.21 0.94 0.27	2.00 0.94 0.28	2.23 0.91 0.51	2.23 0.91 0.51	2.23 0.91 0.51	-	2.38 0.90 0.70



Table 4. Results from Jackknife delete-1 statistics for VPRM estimated domain-wide NEE for different vegetation classes and for all of the land area. The uncertainty in NEE from all land area was derived assuming independence in the vegetation class specific uncertainties. Note the strong asymmetry between the fraction of land area covered by the different vegetation classes and the number of eddy covariance sites used, indicating over/under representation: for example 8 crop sites represent 51% of the land area, while 15 grassland sites represent 5.6% of the land area of Europe.

	NEE [GtC/y]	NEE uncertainty [GtC/y]	Number of sites	Fraction of land area [%]
Evergreen forest	-0.165	0.039	16	16.5
Deciduous forest	-0.174	0.020	5	4.4
Mixed forest	-0.025	0.176	2	8.4
Open shrub ^a	-0.201	-	1	13.8
Savanna ^a	-0.012	-	0	0.3
Crop	-0.443	0.502	8	51.0
Grass	0.059	0.026	15	5.6
Total	0.960	0.536	47	100

^aUncertainties for open shrubland and savanna could not be derived due to the lack of representative eddy covariance sites

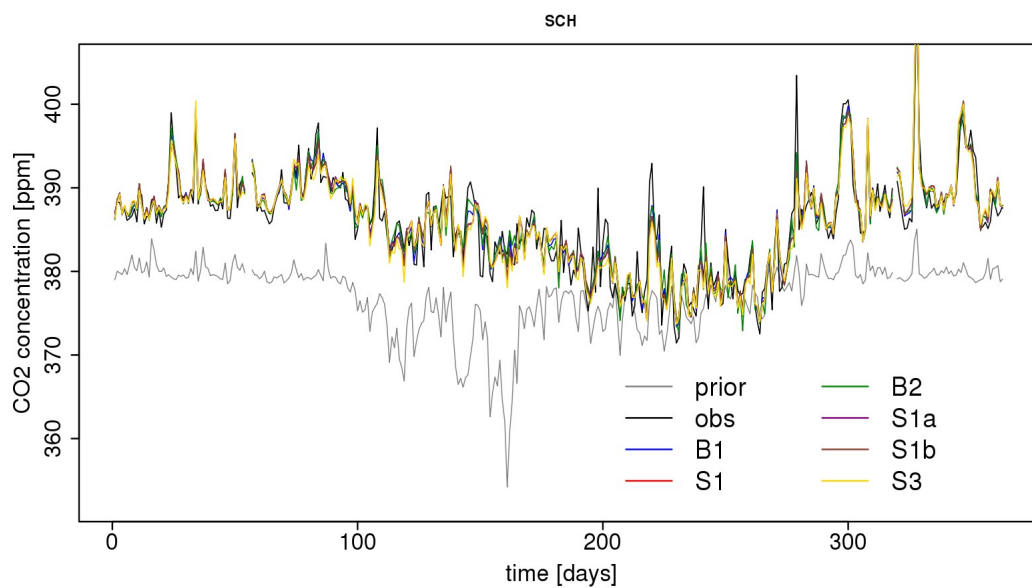


Figure 1. Daily nighttime (23:00-4:00 UTC) averages for prior, true, and posterior CO₂ dry mole fraction time series for the Schauinsland site for the real data inversion. Time starts at 1st January 2007.

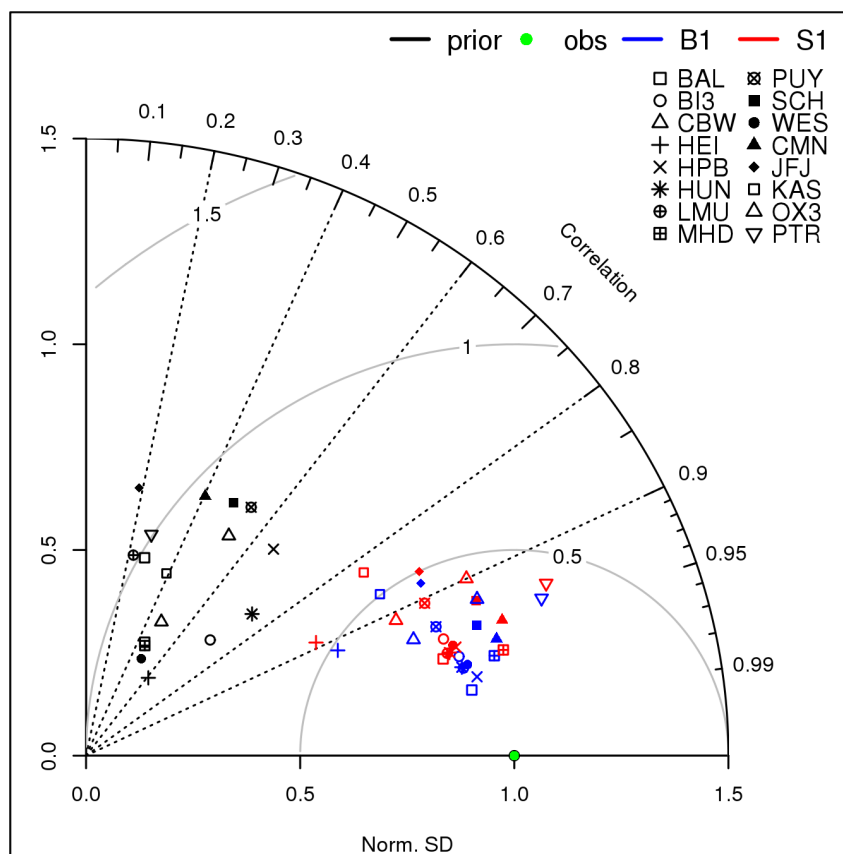


Figure 2 Taylor diagram for modeled and observed time-series of CO₂ dry mole fractions. Prior (black), observed (green, the perfect match of modeled and observed time-series) and the different inversion cases (B1 blue; S1 red) are displayed. Different symbols denote different atmospheric stations. The normalized SD was calculated as the ration of the SD of the modeled time-series to the SD of observations. Gray semi-circles show contours of the standard deviation of the model error.

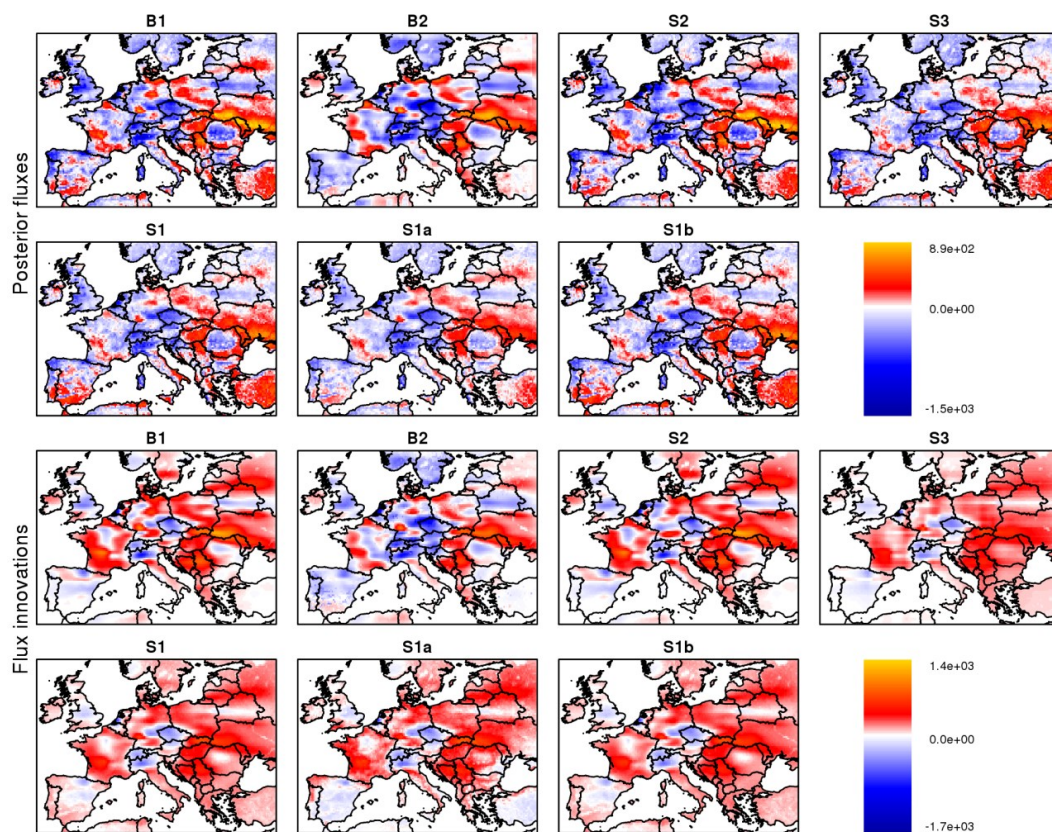


Figure 3. Annual biogenic flux spatial distribution (top two rows) and flux innovations (posterior - prior) (bottom two rows) as estimated from the different inversions for the real data case. Units are in $\text{gCy}^{-1}\text{m}^{-2}$.

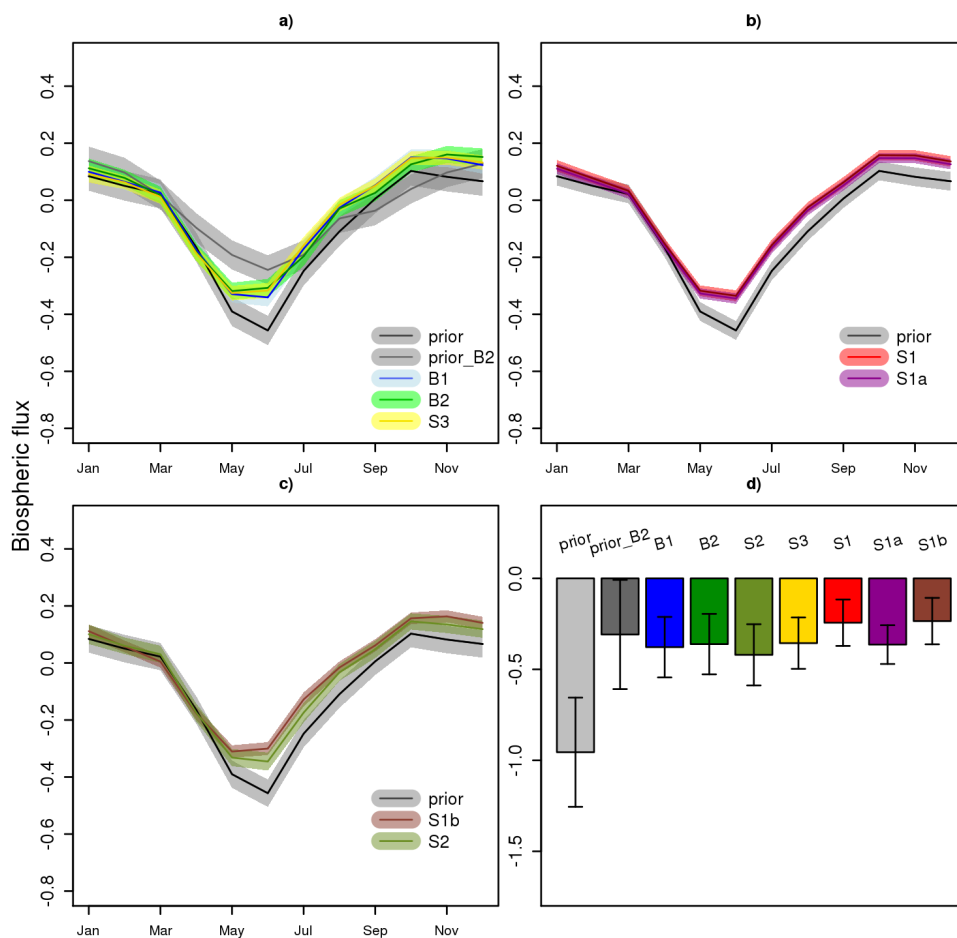


Figure 4. Monthly and annual (panel d) biosphere fluxes integrated over the domain. Panel a) shows B1, B2 and S3 cases, b) S1 and S1a and the c) panel shows S1b and S2 cases. Note that all inversions share the same annual prior uncertainty but monthly prior uncertainties differ. Units are in GtC month^{-1} and GtC y^{-1} for monthly and annual fluxes, respectively

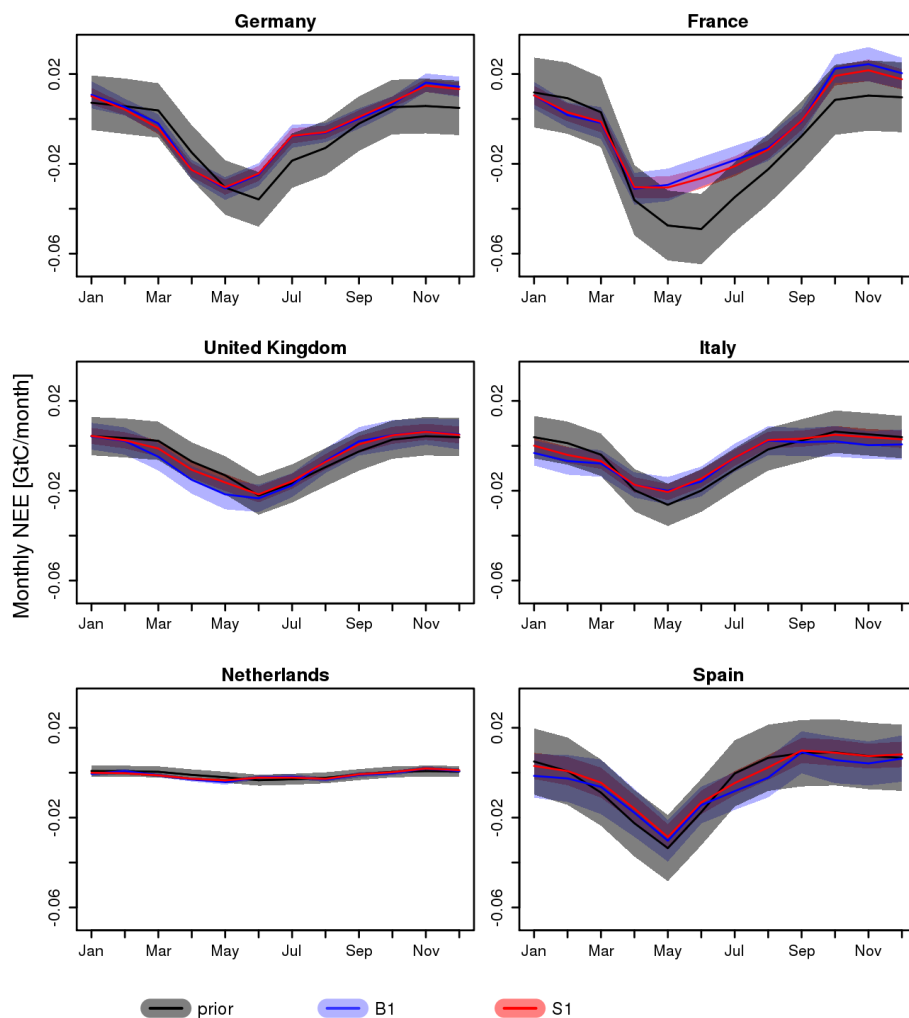


Figure 5. Temporal evolution of prior and posterior monthly NEE for selected European countries.

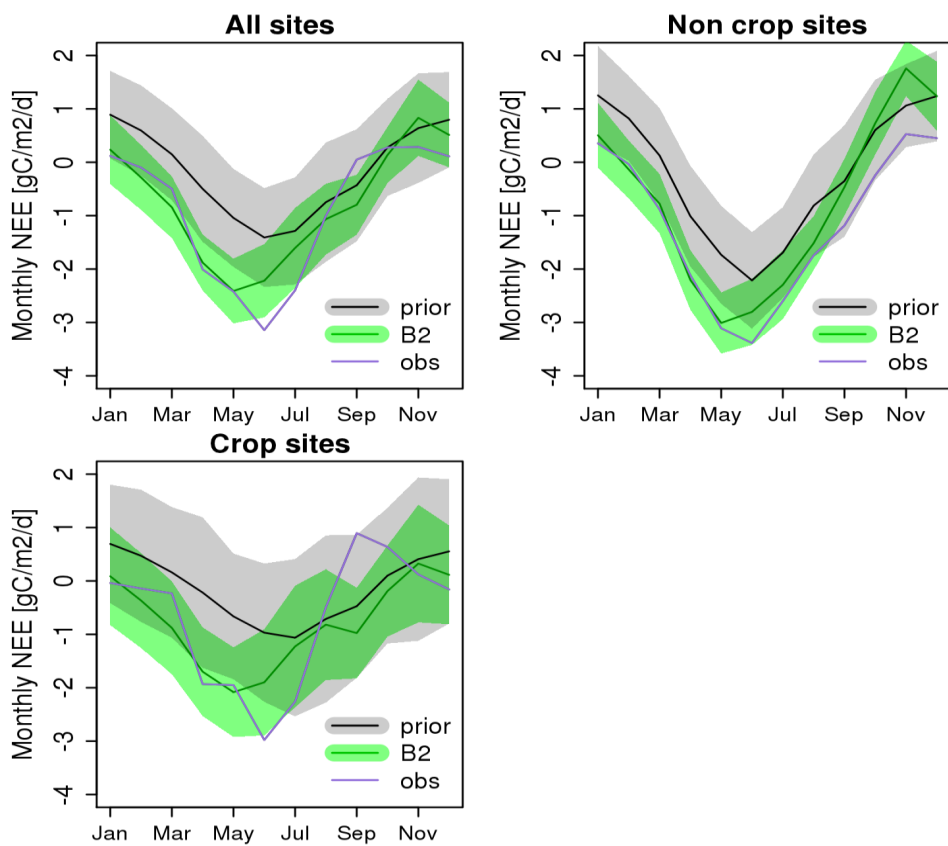


Figure 6. Temporal evolution of monthly NEE ($\text{gCm}^{-2}\text{day}^{-1}$) averaged over all EC sites (top left), excluding crop (top right), and using only crop sites (bottom). Uncertainties (error of the mean monthly NEE) are indicated by the shaded areas.

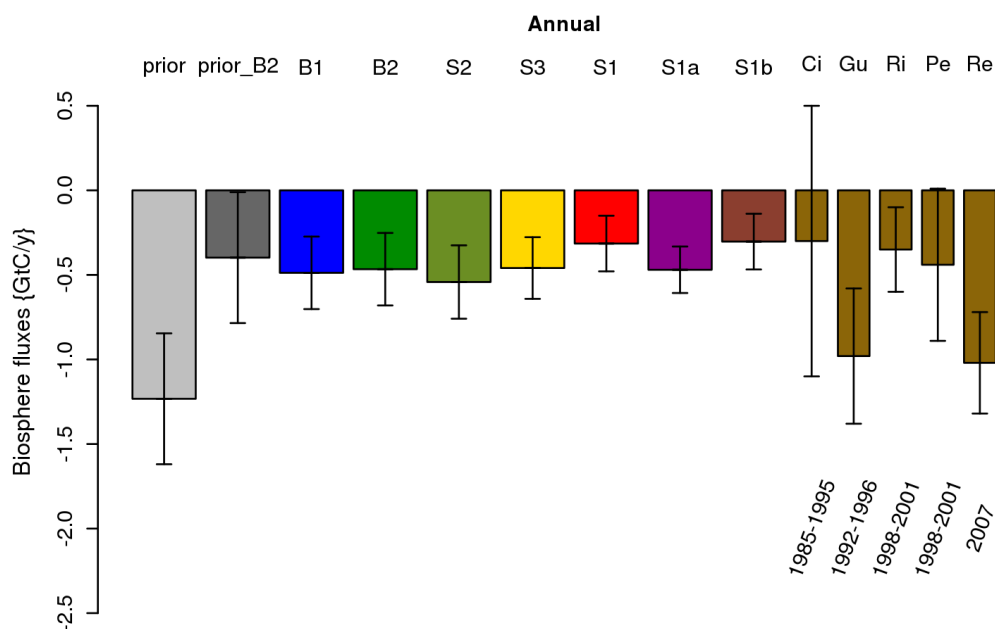


Figure 7. Annual European biogenic CO₂ fluxes in GtC_y⁻¹ for the different inversions and comparison to previous studies. Fluxes are upscaled to the TransCom EU domain. Labels of the references are as follows: Ci : Ciais et al. (2000); Gu : Gurney et al. (2004); Ri : Rivier et al. (2010); Pe : Peylin et al. (2013); Re : Reuter et al. (2014). Periods for the inverted fluxes are given below the flux estimates.